Original Research

Laser Doppler Velocimetry (LDV) and 3D Phase-Contrast Magnetic Resonance Angiography (PC-MRA) Velocity Measurements: Validation in an Anatomically Accurate Cerebral Artery Aneurysm Model With Steady Flow

Dorothea I. Hollnagel, MS,[1] Paul E. Summers, PhD,[2] Spyros S. Kollias, MD,[3] and Dimos Poulikakos, PhD[1]*

Purpose: To verify the accuracy of velocity mapping with three-dimensional (3D) phase-contrast magnetic resonance angiography (PC-MRA) for steady flow in a realistic model of a cerebral artery aneurysm at a 3T scanner.

Materials and Methods: Steady flow through an original geometry model of a cerebral aneurysm was mapped at characteristic positions by state-of-the-art laser Doppler velocimetry (LDV) as well as 3D PC-MRA at 3T. The spatial distributions and local values of two velocity components obtained with these two measurement methods were compared.

Results: The 3D PC-MRA velocity field distribution and mean velocity values exhibited only minor differences to compare to the LDV measurements in straight artery regions for both main and secondary velocities. The differences increased in regions with disturbed flow and in cases where the measurement plane was not perpendicular to the main flow direction.

Conclusion: 3D PC-MRA can provide reliable measurements of velocity components of steady flow in small arteries. The accuracy of such measurements depends on the artery size and the measurement plane positioning.

Key Words: phase mapping; velocity mapping comparison; magnetic resonance angiography (MRA); magnetic resonance imaging (MRI); cerebral aneurysm; laser Doppler velocimetry (LDV)
J. Magn. Reson. Imaging 2007;26:1493–1505.

BASED ON ANGIOGRAPHIC STUDIES, between 3% and 6% of humans harbor intracranial aneurysms, though autopsy studies suggest a slightly lower incidence (1). Approximately 2% of these aneurysms rupture per year and this event is associated with a high mortality and morbidity. Incidentally detected unruptured aneurysms are therefore commonly treated before rupture, either surgically (e.g., by placement of clip during open craniotomy) or endovascularly (e.g., coiling). Understanding and predicting the hemodynamics of unruptured intracranial cerebral aneurysms has potential in aiding safe and efficient treatment by offering important information for therapeutic decision-making and patient management. This can be achieved with numerical simulations based on in vivo patient velocity data acquired with phase-contrast magnetic resonance angiography (PC-MRA), a relatively simple, noninvasive, and adaptable method for performing in vivo blood velocity measurements. Therefore, PC-MRA is attractive as a source of inlet conditions for computational fluid dynamics (CFD). The proposal and first demonstration by Grant and Back (2) and Moran (3), of methods for measuring flow and velocity by phase modulation in combination with MR imaging (PC-MRA) led to the development of both angiographic and quantitative uses of PC-MRA (4–8). Several groups have established PC-MRA for bulk flow measurements (9,10). The quality of the generated computer model however, relies on verifying the accuracy of the PC-MRA as a reliable source of velocity field data.

Comparisons of PC-MRA with numerical simulations (CFD) for steady flow have been limited to relatively large vessels (e.g., carotid artery) (11–13). A good review of combined PC-MRA and CFD is given by Long et al (14). A persistent limitation of evaluating PC-MRA with CFD is that the accuracy of the CFD is not validated for complex geometries like realistic arteries.

Therefore, in the present work, we acquired quantitative three-dimensional (3D) PC-MRA velocity maps of steady flow from a defined, realistic arterial aneurysm

[1]Laboratory of Thermodynamics in Emerging Technologies, ETH Zurich, Zurich, Switzerland.
[2]Department of Neuroradiology, University of Oxford, Radcliffe Infirmary, Oxford, UK.
[3]Institute of Neuroradiology, University Hospital, Zurich, Switzerland.
Contract grant sponsor: Swiss National Science Foundation; Contract grant number: 3200B0-100355.
*Address reprint requests to: D.P., Institute of Energy Technology, LTNT, ETH Zurich, ML J 38, Sonneggstrasse 3, CH-8092 Zurich, Switzerland. E-mail dimos.poulikakos@ethz.ch
Received March 2, 2007; Accepted August 28, 2007.
DOI 10.1002/jmri.21179
Published online 26 October 2007 in Wiley InterScience (www.interscience.wiley.com).

model and compared them with laser Doppler velocimetry (LDV), which is an accepted method in velocity measurement investigations. Comparisons of 2D PC-MRA velocity field maps against LDV have previously been carried out for large diameter (>2.5 cm) and simple models in MR scanners of up to 1.5T, but the PC-MRA results were compared with theoretical values or LDV measurements from other groups (15,16), so that few studies allow direct comparison with LDV measurements on the same model. Nonetheless, Ku et al (15) concluded from measurements of the steady velocity profiles for a variety of flow conditions and simple geometries that PC-MRA is an accurate, noncontacting velocimeter. Siegel et al (16), however, found that steady PC-MRA velocity measurements in areas of stenosis and highly turbulent flow produce a flow error of over 100%. They recommended the use of high signal-to-noise ratios, low echo times, and thick slices to minimize these velocity errors. Tateshima et al (17,18) were able to depict complex 3D intraaneurysmal velocity structures within a scaled up realistic basilar artery tip model with a basilar artery diameter of 10 mm with steady and pulsatile flow in a 1.5T scanner. They emphasized, however, that the equivalent detailed velocity information will be obtainable in vivo only with improvements in spatial resolution.

In keeping with the recommendations of obtaining both high SNR and high resolution in a realistic clinical setting, we have performed 3D PC-MRA of a realistic (in geometry and size) arterial aneurysm model in a high-field 3T MR-scanner to achieve thinner slices and greater SNR than previously reported with 2D PC-MRA studied at 1.5T. We then compared 3D PC-MRA values with LDV measurements performed on the same model, setup, and steady flow rate. A preliminary report on these findings has been made by Hollnagel et al (19,20).

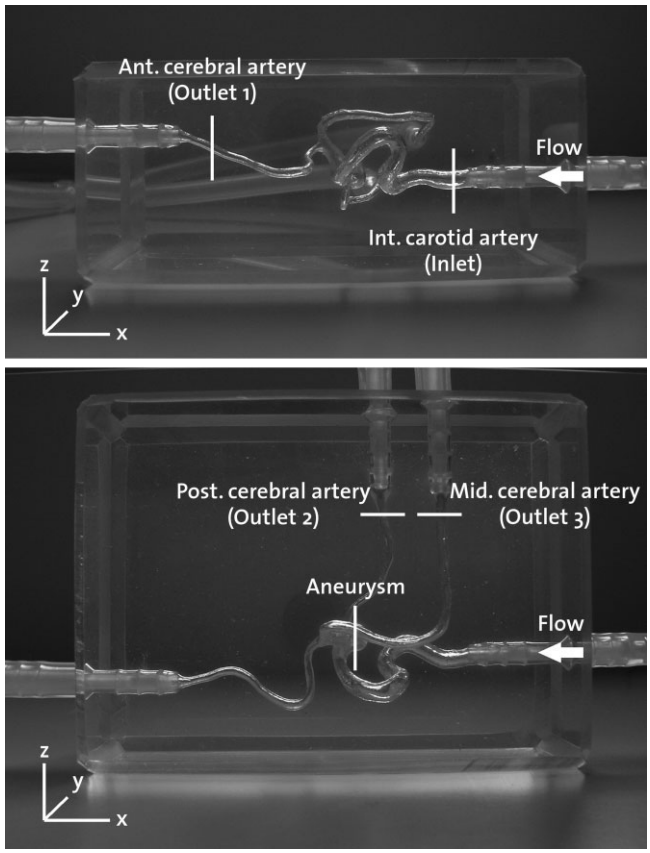

Figure 1. Measurement positions in the model.

MATERIALS AND METHODS

Model and Setup

The geometry for the aneurysm model was segmented from a 3D digital subtraction angiogram of a patient who had provided informed consent to research use. The temporal part of the internal carotid artery at the skull base is the inlet of the model and has a diameter of 3.7 mm to 4 mm. The saccular aneurysm is located at the origin of the posterior communicating artery. The posterior communicating artery passes into the posterior cerebral artery; the very small ophthalmic artery was cut off. Distal to the aneurysm, the internal carotid artery bifurcates into the anterior cerebral artery and the middle cerebral artery. The outlets of the model are therefore the anterior, middle, and posterior cerebral arteries. A stereolithography (.stl) file of the segmented and pruned vascular segment was used to produce a clear silicone model (Sylgard 184; Dow Corning Corporation, Midland, MI, USA) as shown in Fig. 1 (Elastrat Sàrl, Geneva, Switzerland).

A mixture of 59.4% by weight of glycerol in water was used as the blood mimicking fluid. This provided the same refraction index of $N = 1.412$ as the silicone model. Matching the refraction index was of fundamental importance for minimizing the errors due to refraction disturbances for the LDV measurements. Hollow glass spheres with a diameter of 10 μm were added to the fluid as seeding particles for the LDV. The T1 and T2 values of the fluid were measured to be 500 msec and 45 msec, respectively.

The fluid had a density of 1,151.5 kg/m^3 and a viscosity of 10.3 mPa · s. Since the density of blood is 1,050 kg/m^3 (21) and with the assumption that in vivo the viscosity is constant at 4 mPa · s (22–24), the flow had to be adjusted to match in vivo conditions according to the Reynolds analogy (25). An in vivo blood flow rate of 2.3 mL/second in a vessel with a radius of 1.9 mm corresponding to the inlet radius of the model was assumed, yielding a constant Reynolds number of about 200. Under the Reynolds analogy, the constant flow rate through the model was therefore set to 5.4 mL/second.

Accurate and reproducible flow through the model was maintained by using a computer-controlled pump suitable for use in MR environments (CompuFlow 1000 MR; Shelley Medical Imaging Technologies, Mississauga, Canada). This pump is able to generate steady flows with less than 1% variance (26). The vascular model was connected to the pump system via silicone tubes.

Velocity Measurements

The velocity field in the model was measured at the cross-sectional positions indicated by the lines shown

in Fig. 1 for a constant inlet flow of 5.4 mL/second using LDV (Dantec, Skovlunde, Denmark) and 3D PC-MRA (Achieva 3 T; Philips Medical Systems, Best, The Netherlands) with a multichannel head coil.

A long, straight section of tube led to the inlet of the model with the flow and the measurement cross-section parallel to the model boundaries, so that very low secondary velocities are expected. For outlet 2 and outlet 3, the measurement planes were also oriented at approximately right angles to the flow. For outlet 1, however, the measurement cross-section was at significant angles (22° in the xz-plane and 18° in the xy-plane) relative to the flow direction due to geometry (Fig. 1). At the average flow velocity, the length of the tubing on the straight path from the mouth of the scanner bore to the phantom provided 3.5 seconds (equal to 7 × T1 of the fluid) of exposure to the magnetic field, sufficient to provide full polarization for all spins assuming fully developed parabolic flow.

LDV

The principle of the LDV is the Doppler effect (27): the laser acts as a nonmoving transmitter and the particles in the fluid act first as moving receivers, and then as moving transmitters of the reflected light being detected by a nonmoving receiver. The detected light is frequency-shifted relative to that sent from the laser, allowing the velocity of the reflecting particle to be calculated. In practice, this frequency shift is too small to be detected due to the high frequencies involved. Instead, a two-laser-beam setup is used, allowing the velocity component of the reflecting particle in the plane of the beams and perpendicular to the line bisecting the angle between the beams to be calculated from the frequency shift (28,29).

For the LDV measurements in our setup, two argon-ion lasers with two different wavelengths (λ_1 = 514.5 nm [green] and λ_2 = 488 nm [blue]) were used. Each laser beam was split into two beams. The planes spanned by the beams were adjusted perpendicular to each other. With this setup, two velocity components could be measured.

The velocity components were measured at points along radial lines passing through the maximum velocity in each cross-section. The spacing of the points was between 0.05 mm and 0.15 mm and 50,000 velocity samples were acquired per point. The mean of the distribution of these velocity samples was taken to be the velocity at the specific point. This is indicated in the first two pictures in Fig. 2a.

To facilitate the comparison between the LDV and PC-MRA, a cubic interpolation was used to fit a surface to the acquired LDV velocities (Matlab, Version 7.0.1.24704 (R14) service pack 1; The MathWorks, Inc., Natick, MA, USA). The last panels in Fig. 2a show the interpolation from the measured single points to the interpolated surface.

Magnetic Resonance Velocimetry

For the MRA measurements, a standard 3D PC sequence was used with the parameters and resolutions listed in Table 1. The minimum available echo time (TE) was used and the velocity encoding (VENC) was adjusted close to the maximum expected velocity to max-

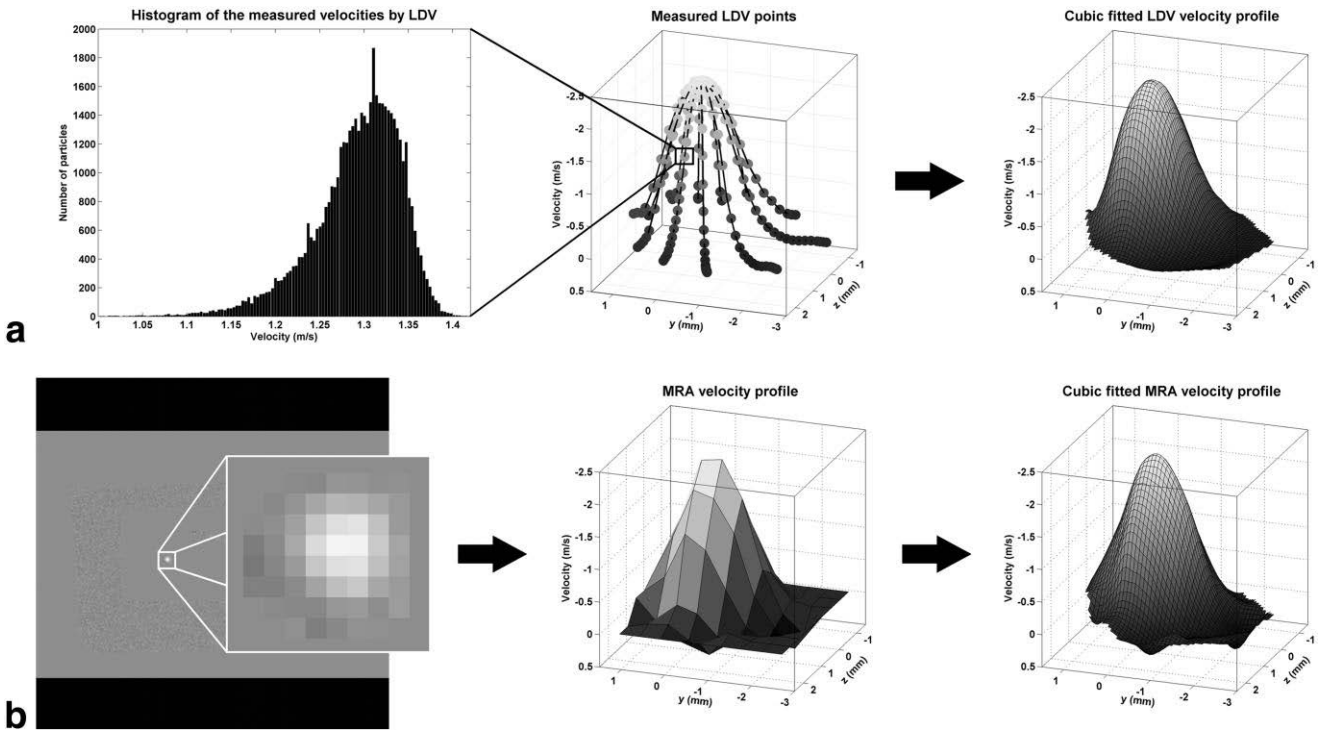

Figure 2. Steps from LDV and PC-MRA data to fitted profiles. **a:** Velocity distributions at several points on specific lines are measured. The mean for each is taken and plotted as a profile. Through the resulting points a surface is fitted. **b:** The ROI is cropped from the PC-MR velocity image. Through the measured points, a surface is fitted.

Table 1
Parameters for the Steady PC-MRA Measurements for the Main and Secondary Velocity Directions

	Inlet	Outlet 1	Outlet 2	Outlet 3	Aneurysm
VENC (cm/second)					
Main direction/secondary direction	300/12	140/70	160/30	175/12	130/90
TE (msec)					
Main direction/secondary direction	4.3/4.8	4.3/4.4	4.2/4.8	4.2/5.5	4.4/4/6
TR (msec)	30	30	30	30	30
Flip angle (°)	8	8	8	8	8
FOV (mm)	150 × 105	150 × 105	150 × 105	150 × 105	150 × 105
Ac Mat (pixels)	320 × 224	320 × 224	320 × 224	320 × 224	320 × 224
Rec Mat (pixels)	320 × 224	320 × 224	320 × 224	320 × 224	320 × 224
Scan %	100	100	100	100	100
NSl	15	15	15	15	19
SlThick (mm)	1	0.7	1	1	0.7
NSA	2	3	3	3	3
Foldover	AP (z)	AP (z)	RL (y)	RL (y)	AP (z)
WFS (pixels)	0.702	0.702	0.702	0.702	0.702
Band (Hz)	618.7	618.7	618.7	618.7	618.7
Time (minutes:seconds)	4:29	6:43	6:43	6:43	8:04

VENC = velocity encoding, TE = echo time, TR = repetition time, FOV = field of view, Ac Mat = acquisition matrix, Rec Mat = reconstruction matrix, Scan % = scan percentage, NSl = number of slices, SlThick = slice thickness, NSA = number of signal averages, Foldover = foldover direction (AP = anterior–posterior, RL = right–left), WFS = water-fat-shift, Band = bandwidth, Time = scan time.

imize the velocity to noise ratio. During the MR measurements the silicone model was placed in an agar gel bath to improve the loading of the MR coils and to provide sufficient static material for the automated tuning and matching.

The MR velocity data was exported from the scanner in Digital Imaging and Communications in Medicine (DICOM) format prior to being preprocessed and visualized in the same way as the LDV data. The interpolated surface was fitted to the PC-MRA data with the same resolution as the LDA surface (Fig. 2b).

With PC-MRA measurements, velocity components in all three directions could be acquired. As noted above, from the LDV measurements, velocity components were obtained only in the main and one secondary direction. Therefore, comparisons were carried out only for these two directions.

Analysis

The velocity maps obtained with 3D PC-MRA and LDV were qualitatively compared at the prescribed cross-sectional locations (Fig. 1) using surface plots for the individual components, and as profiles along the two cardinal directions (cross-lines) of these cross-sections. Between modalities, the interpolated velocity components were individually subjected to correlation analysis for the cross-sections as a whole, and along each of the profiled cross-lines.

To quantitatively compare the LDV and PC-MRA measurements with each other and among each other at the different sites, a rating system was introduced. Different characteristic numbers were obtained:

Correlation coefficient (R), ideal R = 1
Root mean squared error (RMSE) per maximum LDV velocity at the specific site and direction in %, ideal RMSE = 0
Peak velocity difference (PVD) per maximum LDV velocity at the specific site and direction in %, ideal PVD = 0
Mean velocity difference (MVD) per mean LDV velocity at the specific site and direction in %, ideal MVD = 0
Coefficients (m, b) of the standardized regression line: PCMRA′ = LDV′ m + b, ideal m = 1, ideal b = 0 (with PCMRA′ = PCMRA/max. LDV and LDV′ = LDV/max. LDV)

The discrepancies (E) of the characteristic numbers from their ideal values are rated according to the following system:

E ≤ 5%: very good, denoted by ++
5% < E ≤ 10%: + good
10% < E ≤ 15%: – weak
E > 15%: – – poor

For the evaluation, the mean values of the ratings at the specific sites and directions were calculated and quantitative information about the quality of the measurements was obtained at the different sites in the model.

RESULTS

All measurements were performed within 5 cm of the isocenter to minimize the Maxwell terms, and retrospective gating was used to minimize temporal differences in the background due to eddy currents (30). In regions of interest (ROIs) defined in the surrounding static gel, the mean difference and standard deviation (SD) from zero phases corresponded to less than 1.5% and 3.5% of the VENC, respectively; therefore, no measures were taken to further reduce these effects.

Inlet

The PC-MRA and LDV results for the main velocity direction (x) at the inlet (internal carotid artery) are

shown in Fig. 3. The velocity profiles in Fig. 3a are qualitatively similar. There was very little difference between the methods in both the mean velocity and the peak velocity, with the PC-MRA showing a 2.493% (0.012 m/second) lower mean velocity and a 0.244% (0.006 m/second) lower peak velocity compared to the LDV as shown in Table 2. The flow region and the artery size were imaged precisely and the zone of backflow was reproduced with the PC-MRA measurements. In the contour plots (Fig. 3b), the velocity profiles show the same pattern in the main stream, although in the backflow region the absolute velocity was overestimated with PC-MRA. The contour plots also show matching of the size of the artery.

In the scatter plot of all velocity pairs from the LDV and PC-MRA measurements (Fig. 3c), one can see that the velocity pairs distribute around the line of identity. The regression analysis shows a very high correlation coefficient (R = 0.976) with the standardized regression line being PCMRA′ = 0.996 LDV′ + 0.005. The small standard error (RMSE = 6.792%, 0.152 m/second) also confirms the accuracy of the PC-MRA measurements. The dispersion of PC-MRA values around the zero velocity corresponds in part to the PC-MRA overestimation of the backflow noted in the contour plots. It also shows the impact of partial volume effects, limited resolution, and therefore interpolation producing nonzero wall velocities with PC-MRA. In addition, refraction errors from the LDV at places near the artery wall could play a role.

The profiles of the velocity values along cross-lines through the flow region (corresponding to y = 0, z = 0, in the graphs in Fig. 3a and b) were plotted in Fig. 3d. These velocity profiles again demonstrate close agreement of the two measurement methods for the forward velocities, and the overestimation of the backflow by PC-MRA. The correlation coefficients are still higher than in the entire region of analysis (Table 2).

The analysis of the secondary velocity component (z) is shown in the right-hand column in Fig. 3. We note that it was not possible to obtain secondary velocities from the entire flow area with the LDV. The analysis and display for both PC-MRA and LDV are limited to the area for which values were available in both techniques. The velocity profiles (Fig. 3e) show again a very good qualitative agreement between the measurement techniques despite the absolute velocities being very low. The differences in peak and mean velocity (PVD = 11.746%, 0.007 m/second, and MVD = 13.863%, 0.003 m/second; Table 2) are significantly higher than for the main velocity direction. The contour plots clearly show similar flow features (Fig. 3f). The subtle differences in the contours however give rise to a small number of outliers in the scatter plot (Fig. 3g). Regression analysis shows a rather weak correspondence between the measurement methods (R = 0.862, PCMRA′ = 1.247 LDV′ + 0.115), and a poor standard error (RMSE = 23.507%, 0.014 m/second). We note, however, that the absolute velocities involved are roughly one-twentieth of those for the main velocity direction.

The velocity profiles along the cross-lines again show similar general conformations. Although there are small discrepancies in the profiles between the lines, the patterns demonstrated are the same. This similarity is reinforced by the high correlation coefficients for velocities at points on the lines.

Outlet 1

The analyses of the main (x) and secondary (z) velocity directions of PC-MRA and LDV at the horizontal outlet (anterior cerebral artery) are shown in Fig. 4. Similarity is seen in the velocity profiles, but velocity underestimation by the PC-MRA measurements is apparent. The peak and MVDs between the methods for the main direction are only 9.601% (0.125 m/second) and 9.057% (0.058 m/second), but rise to 25.739% (0.171 m/second) and 30.091% (0.108 m/second), respectively, for the secondary velocities (Table 2). In both, the main and secondary directions, the velocity was underestimated by PC-MRA as compared to LDV.

In the contour plots of the velocity profiles the similarity of both measurement methods is again clear, but PC-MRA do not show as detailed velocity patterns as the contour lines of LDV, especially in the center of the flow region.

In the scatter plot of all velocity pairs (Fig. 4c and g), although the velocity pairs distribute around the line of identity, the regression lines for the main and secondary velocity directions (PCMRA′ = 0.891 LDV′ – 0.009 and PCMRA′ = 0.877 LDV′ + 0.096, respectively) are slightly shifted and distorted from the ideal line. Nonetheless, the correlation coefficients of R = 0.907 and R = 0.874 are still high.

The cross-line plots again show the tendency of PC-MRA to underestimate the velocities and poorly map the detailed flow, but the discrepancies are more pronounced than for the inlet.

Outlet 2 and Outlet 3

For the main (z) velocities at the outlets 2 and 3 (posterior cerebral artery and middle cerebral artery) shown on the left-hand sides in Figs. 5 and 6, our observations are similar to those for the inlet. The qualitative agreement is shown in the profile and contour plots. The MVDs and PVDs are low for both cases. The flow region was mapped precisely, even though the sizes of outlets 2 and 3 with diameters between 1.4 mm and 2.4 mm are much smaller than the inlet. The entire region correlation coefficient for outlet 3 is high (R = 0.930), for outlet 2 it is rather low (R = 0.883). The regression lines approach the lines of identity with PCMRA′ = 1.002 LDV′ + 0.134 and PCMRA′ = 0.798 LDV′ – 0.106, for outlets 2 and 3, respectively (Table 2). Whereas the slope of the regression line at the outlet 2 is very close to unity, the line is shifted parallel to the line of identity. In contrast, at the outlet 3 the regression line has a reduced slope, but is less offset. The standard errors are low at outlet 3 (RSME = 8.744%, 0.143 m/second) and rather high at outlet 2 (RSME = 14.327%, 0.23 m/second). The more restricted analyses of velocities along the cross-lines through the flow regions show the same patterns of velocity profiles in the two measurement methods and yield very high correlation coefficients.

The secondary (x) velocity components are shown on the right-hand sides of Figs. 5 and 6. In both cases the

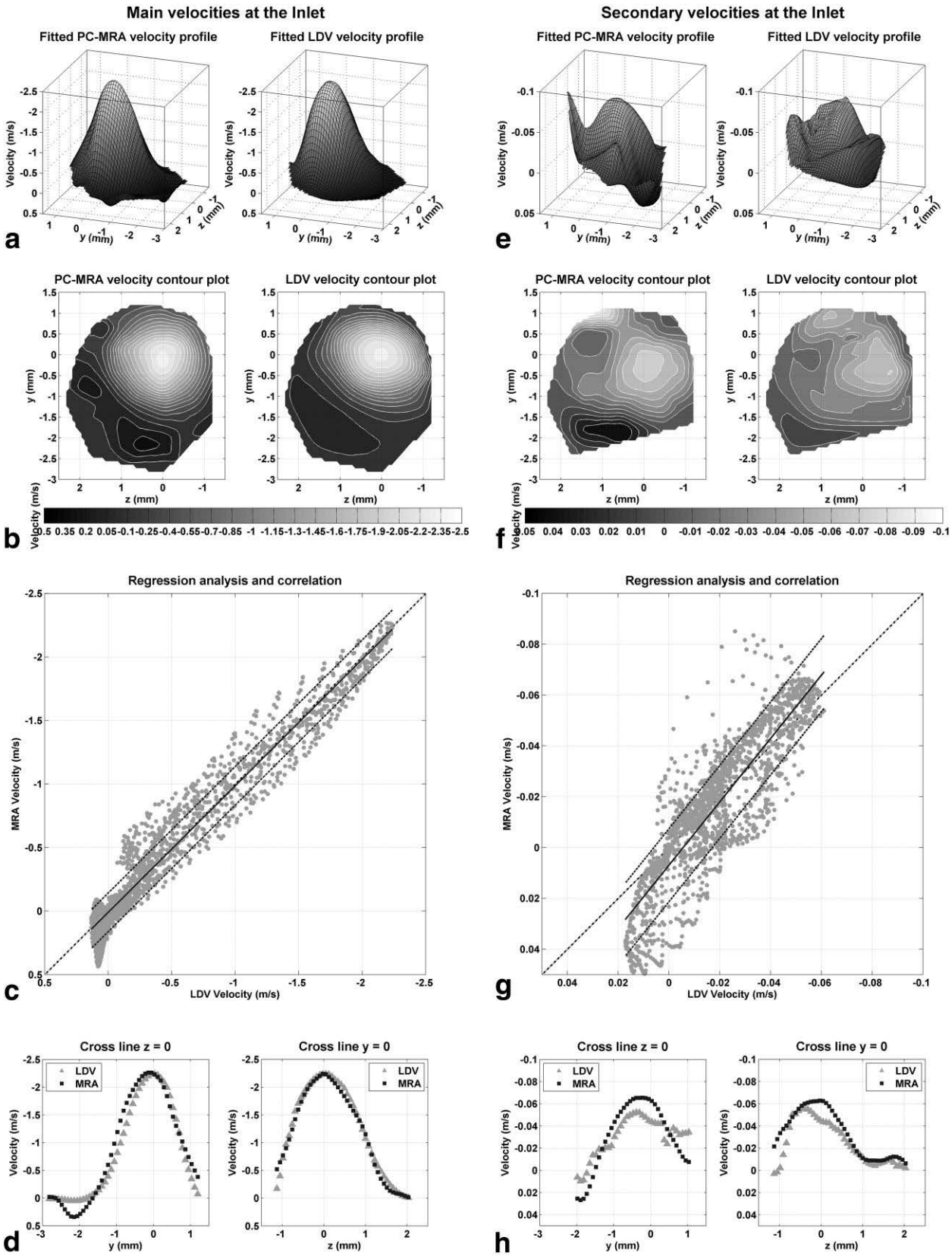

Figure 3. Velocities at the inlet. **a–d:** Main velocities. **e–h:** Secondary velocities. a,e: Velocity profiles, left PC-MRA, right LDV. The qualitative similarity is obvious; the peak and mean velocity differences are minimal. b,f: Contour plots. Same patterns for both methods, though there are differences in the backflow region. c,g: Scatter plots of PC-MRA vs. LDV. Regression analysis shows very high correlation coefficients and regression lines close to the line of identity. d,h: Velocity profiles along cross-lines through the flow region.

Table 2
Data analysis for Entire Region and Lines for Both Flow Directions and the Rating of the Numbers

	Main						Secondary						Σ
	Entire region		Cross-line 1 (z = 0 or x = 0)		Cross-line 2 (y = 0)		Entire region		Cross-line 1 (z = 0 or x = 0)		Cross-line 2 (y = 0)		
Inlet	Value	Rating	Value	Rating	Value	Rating	Value	Rating	Value	Rating	Value	Rating	
R	0.976	+ +	0.977	+ +	0.993	+ +	0.862	−	0.914	+	0.924	+	
RMSE (%)	6.792	+	8.987	+	4.086	+ +	23.507	− −	23.497	− −	14.747	−	
PVD (%)	−0.244	+ +	−0.244	+ +	−0.244	+ +	−11.746	−	24.886	− −	5.170	+	
MVD (%)	−2.493	+ +	5.777	+	−3.075	+ +	−13.863	−	4.024	+ +	34.039	− −	
m	0.996	+ +	1.041	+ +	0.966	+ +	1.247	− −	1.543	− −	0.989	+ +	
b	0.005	+ +	−0.006	+ +	−0.002	+ +	0.115	−	0.290	− −	−0.157	− −	
Σ/n	+1.83		+1.67		+2		−1.33		−0.83		−0.17		
Σ/n			+1.83						−0.78				+0.53
Outlet 1													
R	0.907	+	0.968	+ +	0.985	+ +	0.874	−	0.964	+ +	0.936	+	
RMSE (%)	12.905	−	9.424	+	4.107	+ +	12.825	−	8.817	+	9.125	+	
PVD (%)	−9.601	+	−9.601	+	−9.601	+	−25.739	− −	−18.980	− −	−14.176	−	
MVD (%)	−9.057	+	−5.872	+	−9.592	+	−30.091	− −	−28.627	− −	−27.901	− −	
m	0.891	−	1.147	−	0.725	− −	0.877	−	1.246	− −	0.846	− −	
b	−0.009	+ +	0.112	−	−0.130	−	0.096	+	0.333	− −	0.092	+	
Σ/n	+0.5		+0.5		+0.5		−1		−0.83		−0.33		
Σ/n			+0.5						−0.72				−0.11
Outlet 2													
R	0.883	−	0.921	+	0.998	+ +	0.660	− −	0.732	− −	0.812	− −	
RMSE (%)	14.327	−	14.546	−	2.158	+ +	52.330	− −	58.229	− −	45.331	− −	
PVD (%)	−3.62	+ +	−3.624	+ +	−3.624	+ +	−4.191	+ +	9.221	+	65.490	− −	
MVD (%)	−27.254	− −	−30.741	− −	1.446	+ +	50.146	− −	−28.292	− −	57.891	− −	
m	1.002	+ +	1.208	− −	0.960	+ +	1.009	+ +	0.975	+ +	1.764	− −	
b	0.134	−	0.311	− −	−0.036	+ +	0.034	+ +	−0.026	+ +	0.105	−	
Σ/n	−0.17		−0.67		+2		0		−0.17		−1.83		
Σ/n			+0.39						−0.67				−0.14
Outlet 3													
R	0.930	+	0.973	+ +	0.959	+ +	0.914	+	0.944	+	0.911	+	
RMSE (%)	8.744	+	6.611	+	7.106	+	9.257	+	9.247	+	8.691	+	
PVD (%)	−7.903	+	−7.903	+	−7.903	+	−47.006	− −	−15.892	− −	−42.438	− −	
MVD (%)	3.844	+ +	−9.983	+	2.930	+ +	−29.525	− −	−25.168	− −	−43.656	− −	
m	0.798	− −	0.936	+	0.789	− −	0.751	− −	0.679	− −	0.731	− −	
b	−0.106	−	0.021	+ +	−0.153	− −	−0.018	+ +	0.035	+ +	−0.099	+	
Σ/n	+0.33		+1.33		+0.33		−0.33		−0.33		−0.5		
Σ/n			+0.67						−0.39				+0.14
Aneurysm													
R	0.854	−	0.791	− −	0.926	+	0.741	− −	0.764	− −	0.245	− −	
RMSE (%)	21.522	− −	10.792	−	18.408	− −	25.875	− −	97.472	− −	86.062	− −	
PVD (%)	−28.621	− −	−28.621	− −	−28.621	− −	−7.966	+	−65.247	− −	−68.647	− −	
MVD (%)	−0.002	+ +	42.288	− −	146.48	− −	49.193	− −	−110.24	− −	30.239	− −	
m	0.897	−	0.480	− −	1.028	+ +	1.015	+ +	2.536	− −	0.411	− −	
b	−0.091	+	−0.340	− −	−0.031	+ +	0.086	+	−1.258	− −	0.074	+	
Σ/n	−0.5		−1.83		−0.17		−0.33		−2		−1.5		
Σ/n			−0.83						−1.28				−1.06

R = correlation coefficient, RMSE = root mean squared error, PVD = peak velocity difference, MVD = mean velocity difference, m = slope, b = intercept of regression line (PCMRA′ = m LDV′ + b). Ratings of discrepancies (E) of the characteristic numbers: E ≤ 5%: very good: + +, 5% < E ≤ 10%: good: +, 10% < E ≤ 15%: Weak: −, E > 15%: poor. − −

flow patterns measured with the different methods are similar but agreement on the absolute values of the velocities is rather poor. For the entire region regression analyses and the cross-line analyses, high correlation coefficients were obtained for outlet 3, but only poor correlation coefficients for outlet 2. The regression lines for the secondary velocities at these outlets are similar to the lines for the main velocities. The secondary velocity regression line for outlet 2 (PCMRA′ = 1.009 LDV′ + 0.034) is close to the line of identity, while the slope of the regression line at the outlet 3 (PC-MRA′ = 0.751 LDV′ – 0.018) is reduced but the line is not offset.

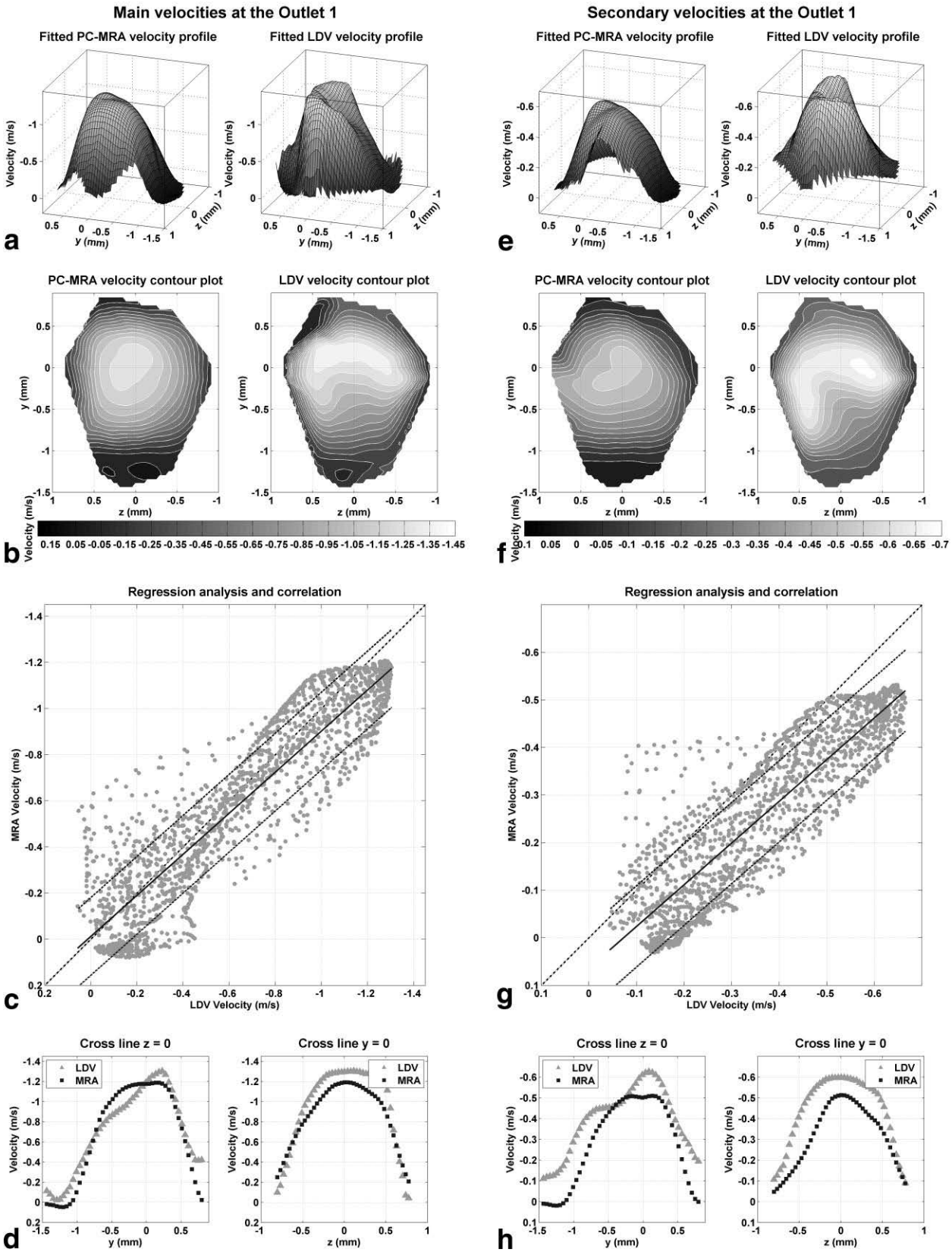

Figure 4. Velocities at the outlet 1. **a–d:** Main velocities. **e–h:** Secondary velocities. a,e: Velocity profiles, left PC-MRA, right LDV. Although qualitatively similar profiles are obtained, velocity underestimation by PC-MRA is apparent. b,f: Contour plots of PC-MRA do not show as detailed patterns as the LDV plots. c,g: Scatter plots of PC-MRA vs. LDV. Regression analysis shows high correlation coefficients and slightly shifted and distorted regression lines to the line of identity. d,h: Velocity profiles along cross-lines through the flow region show underestimation of PC-MRA.

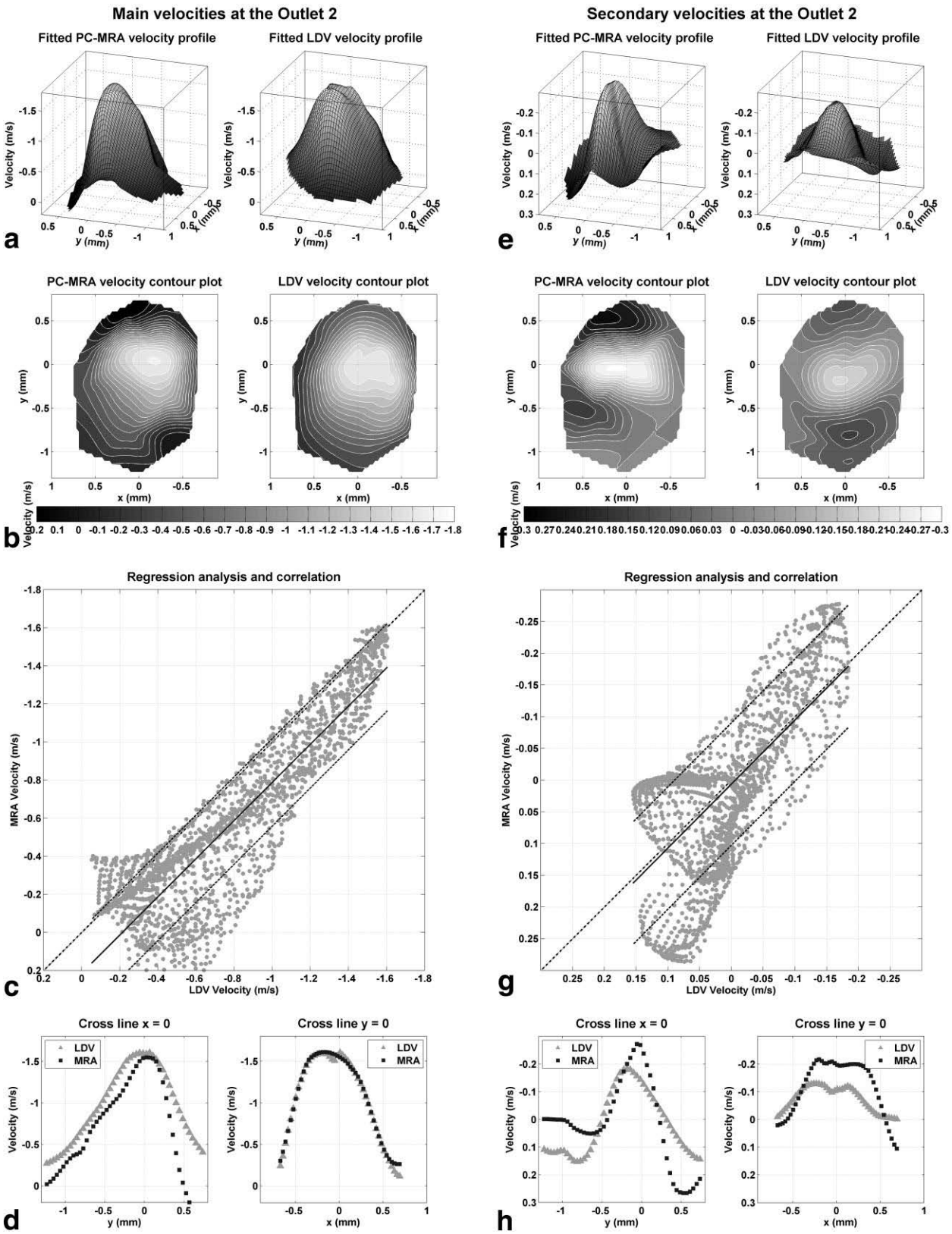

Figure 5. Velocities at the outlet 2. **a–d:** Main velocities. **e–h:** Secondary velocities. a,e: Velocity profiles, left PC-MRA, right LDV. Qualitatively similar profiles, the peak and mean velocity differences are small for the main velocity, but significant for the secondary velocity. b,f: Contour plots show the same patterns for the main velocity component, but differences for the velocity component. c,g: Scatter plots of PC-MRA vs. LDV. Regression analysis shows high correlation coefficients and regression lines with slopes close to unity but shifted. d,h: Velocity profiles along cross-lines through the flow region.

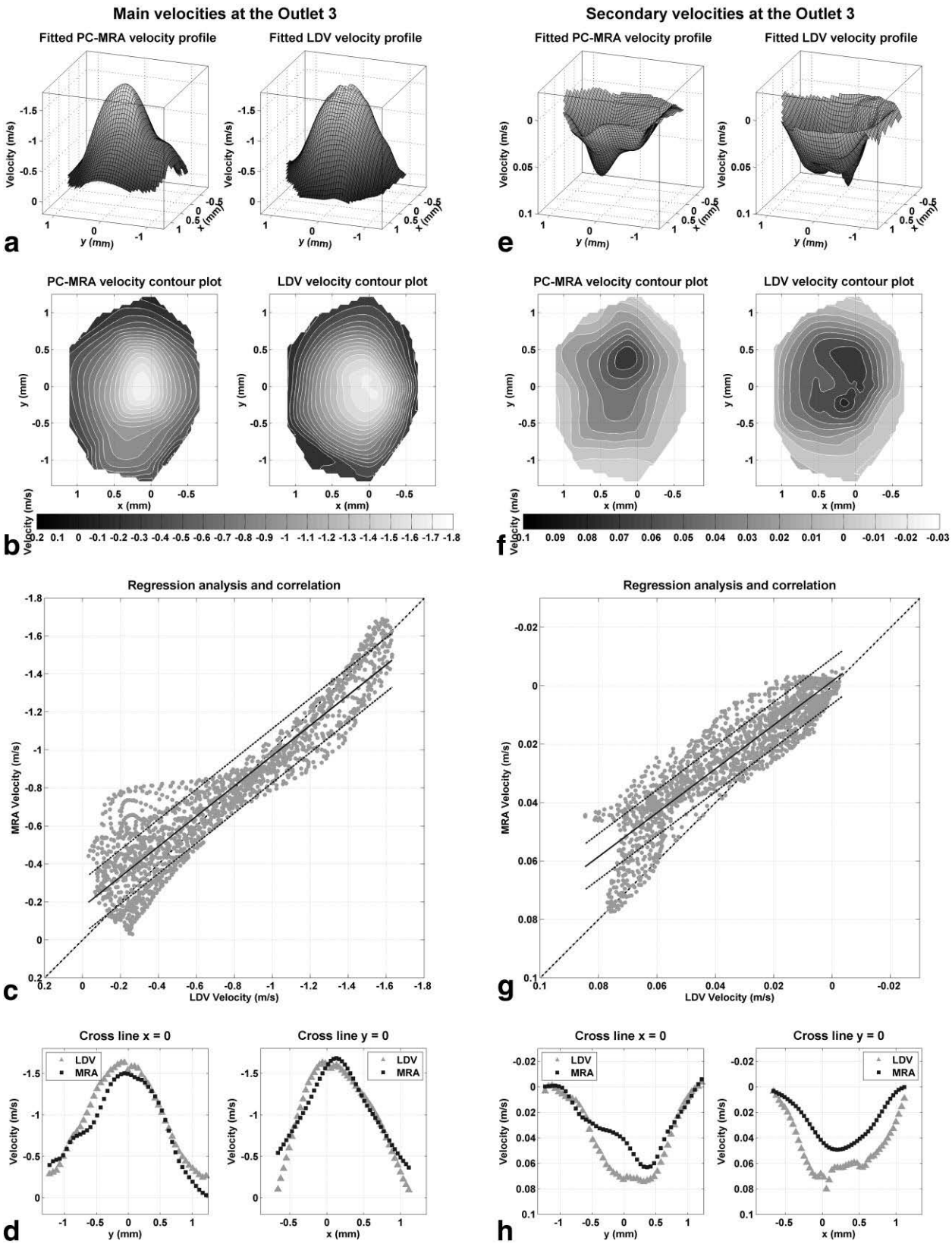

Figure 6. Velocities at the outlet 3. **a–d:** Main velocities. **e–h:** Secondary velocities. a,e: Velocity profiles, left PC-MRA, right LDV. Same profile patterns, especially for the main flow direction. Peak and mean velocity differences are minimal for the main velocities, rather high for the secondary. b,f: Contour plots. Similar patterns for both methods for the main velocities, differences for the secondary velocities. c,g: Scatter plots of PC-MRA vs. LDV. Regression analysis shows high correlation coefficients and regression lines with reduces slopes, but not shifted. d,h: Velocity profiles along cross-lines through the flow region.

Aneurysm

The analysis of the main (x) velocity in the aneurysm is shown on the left-hand side of Fig. 7. The velocity profiles and the contour plots show similar flow patterns for the PC-MRA and LDV measurements, with the MVD being very low. On the other hand, the PVD and the correlation coefficient (R = 0.854) are rather weak (Table 2). The differences noted in the velocity patterns tend to be in the smaller features and may reflect the lower resolution of the PC-MRA images. Although the variance is rather high (RSME = 21.522%, 0.2 m/second), the regression line PCMRA′ = 0.897 LDV′ – 0.091 corresponds to the line of identity.

Similar observations hold for the secondary (z) velocities shown on the right-hand side in Fig. 7. The velocity patterns are the same and despite the very low correlation coefficient (R = 0.741) and the high variance (RSME = 25.875%, 0.119 m/second), the regression line PCMRA′ = 1.015 LDV′ + 0.086 fits well to the line of identity.

DISCUSSION

To obtain accurate results, Tang et al (31) recommend ensuring that the flow region is covered by at least 16 isotropic voxels to minimize partial volume effects within the flow region. This recommendation was fulfilled for the PC-MRA measurements at the inlet, outlet 3, and the aneurysm, though not for outlet 1 (nine voxels) and outlet 2 (12 voxels). Consistent with this, the best match (rating = +0.53) was observed at the inlet, where the diameter of the artery was the largest and the measurement was taken in an almost straight vessel region with the measurement plane placed perpendicular to the main velocity direction. Also, in outlet 3, with a diameter about half that of the inlet, good results (rating: +0.14) were achieved with measurement planes perpendicular to the main velocity direction. For outlet 2, however, the measurement plane was not perfectly adjusted and the flow area could only be covered with 12 voxels, so that the results were poorer (rating = –0.14) than at the inlet and outlet 3. For outlet 1 the measurement plane showed significant angles (22° in the xz-plane and 18° in the xy-plane) between the imaging plane and the artery's main flow direction, and despite the artery's diameter being significantly higher than for the outlets 2 and 3, the flow region could only be covered with nine voxels, so that the accuracy obtained in the velocity patterns at this site was low (rating = –0.11).

Vessel-slice obliquity is a recognized source of partial volume effects as described (31), with the severity dependent on vessel size and the voxel dimensions of the image. This is a probable explanation for the poor performance in outlet 1, which was measured with a significant angle between the imaging plane and the artery's main flow direction. The imaging plane for outlet 2 was not perfectly perpendicular to the artery, and may similarly account for the greater dispersion seen in the scatter plots for this vessel, particularly for the secondary component, compared to outlet 3. The relevance for in vivo situations, where most vessels, particularly small ones, exhibit curvature over even a few millimeters, of avoiding these partial volume errors, is probably limited.

Within the aneurysm, poor quantitative agreement (rating = –1.06) was obtained, though good qualitative agreement was gained for the conformation of the velocity pattern, even though the aneurysmal sac is a region of highly disturbed flow. This produces rather high velocity components in all three directions with a strong three dimensional structure. Thus, the imaging plane cannot be ensured to be perpendicular to the flow throughout the cross-section of the aneurysm. The above mentioned partial volume effects, together with displacement artifacts due to the non-simultaneity of spatial encoding in PC-MRA, as described by Steinman et al (32) can be expected to limit the accuracy of velocity measurements in the intraaneurysmal flow. Consequently, even with the minimum possible slice thickness of 0.7 mm used here, it is rather difficult and time consuming to develop a full 3D velocity profile suitable for making a precise statement on the velocity patterns in small to middle sized aneurysms like in this model with dimensions of about 7 × 5 × 5 mm.

An important factor in maximizing the velocity to noise ratio is the choice of VENC. We have individually chosen the VENC for each measured direction to be high enough to avoid phase wrapping. To improve the velocity SNR, an alternative would have been to use smaller VENCs and to unwrap the phases as a postprocessing step. However, in an aneurysm and for the secondary velocity components in general, the directions of the components are not known beforehand, and may be sufficiently complex to lead to an intractable phase unwrapping problem. Multiple measurements performed with a higher VENC to determine the general direction and a lower VENC may have reduced the noise, but would have extended the already long measurement times.

The observations from the method comparisons can be summarized as follows:

1. 3D PC-MRA provides good results for main flow measurements in straight arteries when the plane of measurement plane is perpendicular to the vessel direction.
2. 3D PC-MRA gives reasonable results for low in-plane velocities for the same case.
3. 3D PC-MRA gives qualitatively reasonable results also for single planes in highly disturbed regions, but it is very difficult and time consuming to gain full 3D velocity profiles in these areas.

In this study one special saccular aneurysm case was examined. Saccular aneurysms are the most common aneurysms in the area of the circle of Willis and are of the greatest interest for the practice of endovascular treatment. Thus, while not presenting the same details we might expect to see in other aneurysms (e.g., fusiform), the present work provides a signpost in the development of MR phase mapping. The findings showed that the measurements in the feeding arteries provide accurate results. These should not be influenced by the form of the aneurysm in between. Measurements within the aneurysm however, showed rather poor de-

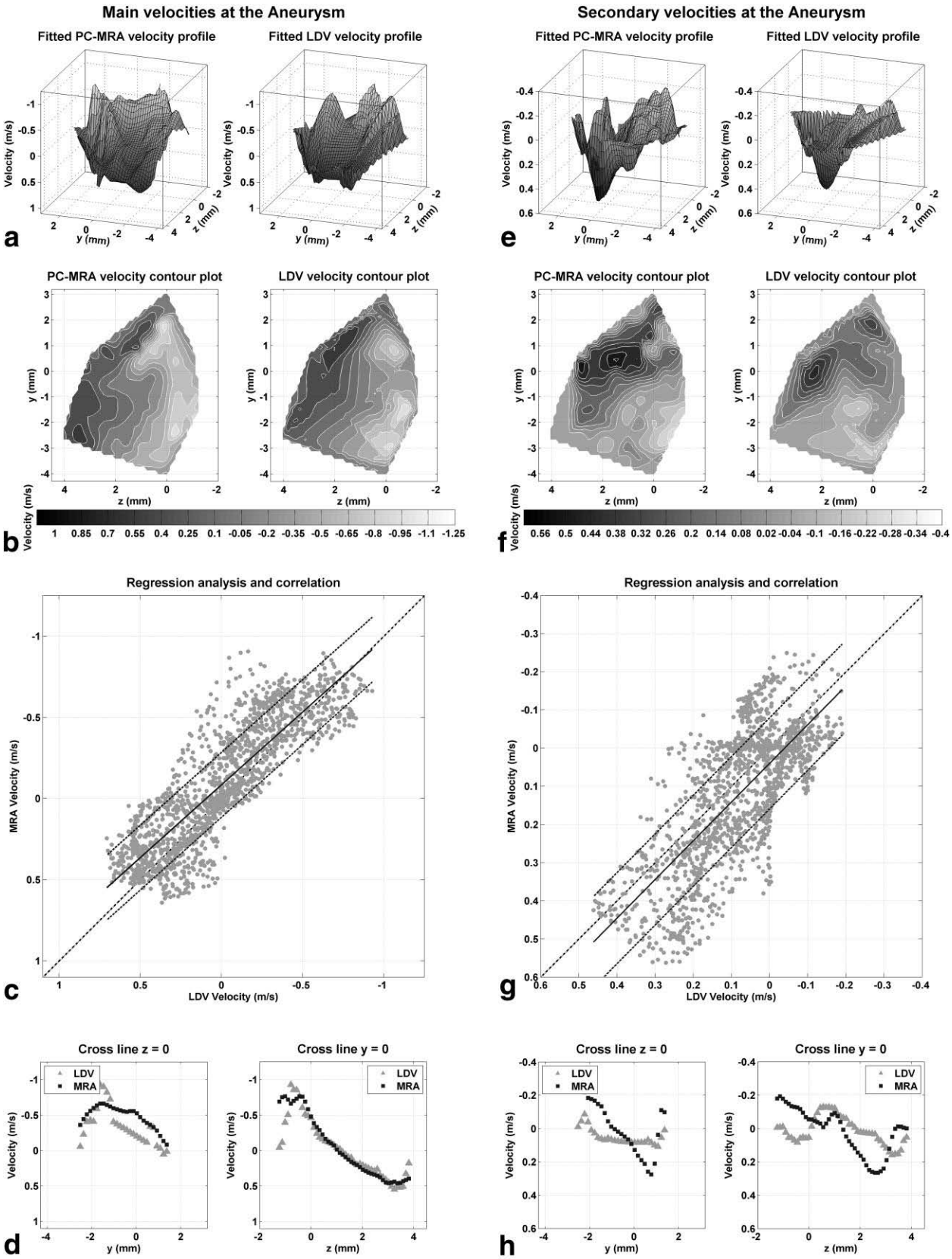

Figure 7. Velocities in the aneurysm. **a–d:** Main velocities. **e–h:** Secondary velocities. a,e: Velocity profiles, left PC-MRA, right LDV. Qualitatively similar patterns. MVDs are minimal for the main velocities, but increasing for the secondary ones. b,f: Contour plots. Similar patterns for both methods. c,g: Scatter plots of PC-MRA vs. LDV. Regression analysis shows relatively high correlation coefficients and regression lines close to the line of identity. d,h: Velocity profiles along cross-lines through the flow region.

piction of the complex flow patterns, which are likely to be more or less distinctive for different aneurysmal sac geometries.

In conclusion, 3D PC-MRA provides indicative measures of velocity components of steady flow in small arteries with differing degrees of accuracy. We found the velocity profiles on different sites in the model to show strong similarities between the 3D PC-MRA and the gold-standard LDV method as evidenced by the high correlation coefficients and regression lines being close to the lines of identity. Still to be examined though, is the quality of MR in the presence of pulsatile physiological flow. The underlying interest in high accuracy of PC-MRA, even in small arteries, is to understand the limits of the method when used to acquire original patient-specific data easily and noninvasively for the formation of patient-specific computer models. These models can then be used to simulate the patient-specific flow and velocities through the parent artery geometry and within the aneurysms, thus providing reliable hemodynamic information that would aid in the prediction of future aneurysmal behaviors and the planning of appropriate therapeutic strategies.

ACKNOWLEDGMENTS

Dr. Lars Blum, Laboratory of Thermodynamics in Emerging Technologies (LTNT), ETH Zurich, provided assistance with the LDV. Dr. Roger Lüchinger, Institute for Biomedical Engineering (IBT), ETH Zurich, kindly helped with the MR scanner. Dr. Makoto Ohta, University Hospital Geneva (HUG), supplied the angiographic data.

REFERENCES

1. Rinkel GJ, Djibuti M, Algra A, van Gijn J. Prevalence and risk of rupture of intracranial aneurysms: a systematic review. Stroke 1998;29:251–256.
2. Grant JP, Back C. NMR rheotomography: feasibility and clinical potential. Med Phys 1982;9:188–193.
3. Moran PR. A flow velocity zeugmatographic interlace for NMR imaging in humans. Magn Reson Imaging 1982;1:197–203.
4. Redpath TW, Norris DG, Jones RA, Hutchison JM. A new method of NMR flow imaging. Phys Med Biol 1984;29:891–895.
5. Bryant DJ, Payne JA, Firmin DN, Longmore DB. Measurement of flow with NMR imaging using a gradient pulse and phase difference technique. J Comput Assist Tomogr 1984;8:588–593.
6. Nayler GL, Firmin DN, Longmore DB. Blood flow imaging by cine magnetic resonance. J Comput Assist Tomogr 1986;10:715–722.
7. Walker MF, Souza SP, Dumoulin CL. Quantitative flow measurement in phase contrast MR angiography. J Comput Assist Tomogr 1988;12:304–313.
8. Firmin DN, Nayler GL, Kilner PJ, Longmore DB. The application of phase shifts in NMR for flow measurement. Magn Reson Med 1990; 14:230–241.
9. Spilt A, Box FM, van der Geest RJ, et al. Reproducibility of total cerebral blood flow measurements using phase contrast magnetic resonance imaging. J Magn Reson Imaging 2002;16:1–5.
10. Zananiri FV, Jackson PC, Goddard PR, Davies ER, Wells PN. An evaluation of the accuracy of flow measurements using magnetic resonance imaging (MRI). J Med Eng Technol 1991;15:170–176.
11. Botnar R, Rappitsch G, Scheidegger MB, Liepsch D, Perktold K, Boesiger P. Hemodynamics in the carotid artery bifurcation: a comparison between numerical simulations and in vitro MRI measurements. J Biomech 2000;33:137–144.
12. Köhler U, Marshall I, Robertson MB, Long Q, Xu XY, Hoskins PR. MRI measurement of wall shear stress vectors in bifurcation models and comparison with CFD predictions. J Magn Reson Imaging 2001;14:563–573.
13. Zhao SZ, Papathanasopoulou P, Long Q, Marshall I, Xu XY. Comparative study of magnetic resonance imaging and image-based computational fluid dynamics for quantification of pulsatile flow in a carotid bifurcation phantom. Ann Biomed Eng 2003;31:962–971.
14. Long Q, Xu XY, Collins MW, Griffith TM, Bourne M. The combination of magnetic resonance angiography and computational fluid dynamics: a critical review. Crit Rev Biomed Eng 1998;26:227–274.
15. Ku DN, Biancheri CL, Pettigrew RI, Peifer JW, Markou CP, Engels H. Evaluation of magnetic resonance velocimetry for steady flow. J Biomech Eng 1990;112:464–472.
16. Siegel JM, Jr., Oshinski JN, Pettigrew RI, Ku DN. The accuracy of magnetic resonance phase velocity measurements in stenotic flow. J Biomech 1996;29:1665–1672.
17. Tateshima S, Grinstead J, Sinha S, et al. Intraaneurysmal flow visualization by using phase-contrast magnetic resonance imaging: feasibility study based on a geometrically realistic in vitro aneurysm model. J Neurosurg 2004;100:1041–1048.
18. Tateshima S, Murayama Y, Villablanca JP, et al. Intraaneurysmal flow dynamics study featuring an acrylic aneurysm model manufactured using a computerized tomography angiogram as a mold. J Neurosurg 2001;95:1020–1027.
19. Hollnagel D, Summers P, Kollias S, Poulikakos D. Comparing steady and pulsatile LDV and PC-MRA flow measurements in an anatomically accurate cerebral artery aneurysm model. In: Proceedings of the 14th Annual Meeting of ISMRM, Seattle, WA, USA, 2006 (Abstract 1919).
20. Hollnagel D, Summers P, Kollias S, Poulikakos D. PC-MRA validation in an anatomically accurate cerebral artery aneurysm model for steady flow. In: Proceedings of the Medical Image Computing and Computer-Assisted Intervention (MICCAI) Workshop Computational Biomechanics for Medicine, Copenhagen, Denmark, October 2006.
21. Kenner T. The measurement of blood density and its meaning. Basic Res Cardiol 1989;84:111–124.
22. Haynes RH. The rheology of blood. Transactions of the Society of Rheology 1961;5:85–101.
23. Merrill EW. Rheology of blood. Physiol Rev 1969;49:863–888.
24. Schmid-Schönbein H, Wells RE, Jr. Rheological properties of human erythrocytes and their influence upon the “anomalous” viscosity of blood. Ergeb Physiol 1971;63:146–219.
25. Reynolds O. An experimental investigation of the circumstances which determine whether the motion of water shall be direct or sinuous, and of the law of resistance in parallel channels. Philos Trans R Soc London 1883;174:935–982.
26. Holdsworth DW, Rickey DW, Drangova M, Miller DJ, Fenster A. Computer-controlled positive displacement pump for physiological flow simulation. Med Biol Eng Comput 1991;29:565–570.
27. Doppler C. On the colored light of the double stars and other heavenly bodies. Abhandl d Kgl Böhm Ges d Wiss 1842:5. pp. 466–483.
28. Durst F, Melling A, Whitelaw JH. Principles and practice of laser-Doppler anemometry. London: Academic Press; 1981. 437 p.
29. DANTEC. Burst Spectrum Analyser, User’s guide. Skovlund, Denmark: DANTEC Electronics; 1990.
30. Bernstein MA, Zhou XJ, Polzin JA, et al. Concomitant gradient terms in phase contrast MR: analysis and correction. Magn Reson Med 1998;39:300–308.
31. Tang C, Blatter DD, Parker DL. Accuracy of phase-contrast flow measurements in the presence of partial-volume effects. J Magn Reson Imaging 1993;3:377–385.
32. Steinman DA, Ethier CR, Rutt BK. Combined analysis of spatial and velocity displacement artifacts in phase contrast measurements of complex flows. J Magn Reson Imaging 1997;7:339–346.